33RD CONGRESS
OF THE INTERNATIONAL COUNCIL
OF THE AERONAUTICAL SCIENCES
STOCKHOLM, SWEDEN, 4-9 SEPTEMBER, 2022

ICAS 2022 SWEDEN

TRANSONIC FLOW OVER DELTA WING USING ENTROPIC LATTICE BOLTZMANN METHOD

Milind Dhake[1], Chakradhar Thantanapally[1], Salvatore Arcidiacono[1] & Santosh Ansumali[1,2]

[1]SankhyaSutra Labs Limited©, Bangalore, India
[2]Jawaharlal Nehru Centre for Advanced Scientific Research, Bangalore, India

Abstract

This work investigates the transonic flow over a 65° swept-back delta wing with a sharp leading edge. The behaviour of vortex breakdown in cross-flow shocks makes the problem setup highly complex in contrast to subsonic vortical flows. It has been reported that increasing the Angle of Attack (AoA) leads to a complex interaction of the strong vortex and shock waves over the wing. To study the onset of the vortex breakdown on the wing in the presence of shocks, we carried out simulations at AoA of 18.6°and 23.6°. The Mach and Reynolds numbers of the simulations are 0.85 and 6×10^6 respectively. The simulations are carried out using the SankhyaSutra Labs©(SSL's) in-house higher order Entropic Lattice Boltzmann Method (ELBM) transonic solver [1]. These results are compared with experimental results reported in the literature[2]. The computed lift coefficient and pressure distribution show good agreement with experiments. The topological aspects of vortex breakdown and its onset in the presence of a system of shocks is discussed.

Keywords: transonic flow, shock vortex interaction, delta wing, vortex breakdown

1. Introduction

Vortex breakdown in a delta wing is accompanied by a sudden change in the pressure distribution which has a detrimental effect on the aerodynamic characteristics such as lift distribution and stall. This forms the motivation for a thorough study of the vortical flows over slender, sharp edge delta wings [3, 4, 5, 6]. Vortex breakdown takes place in the rear portion of the delta wing at higher incidences in subsonic flows as well and is fairly well understood[4, 7, 8]. Transonic flow conditions in delta wings at a moderately high AoA gives rise to complex interactions between shock waves and the leading-edge vortex system. The experimental database from Langley National Transonic Facility (NTF) for transonic flow over a 65° swept-back delta wing can be found in [9]. NTF carried out experiments for a range of Mach and Reynolds numbers and created this comprehensive database which can be used for validations of numerical simulations. The existing literature on transonic flows shows that an increase in Mach number affects the size and shape of the vortex systems [10, 11, 12, 13]. Moreover, the appearance of shock waves further complicates the flow structures. These shock waves are caused by the localised supersonic flow regions over the wing. An analysis of the onset of the vortex breakdown with increasing AoA is explained by Lucy et al [9]. The flow features of interest here are the terminating shock surface at the rear end and the cross-flow shocks present along the leading edge of the delta wing [3]. The pressure distribution on the symmetry plane with increasing AoA, reported from wind tunnel experiments [17], show that the vortex breakdown is observed beyond 22 degrees in addition to a system of shocks already present towards the trailing end of the wing.
The current investigation focuses on capturing the vortex breakdown and shock locations mentioned above. Considering the highly complex nature of this flow, an accurate understanding of these flow features requires a simulation like Large Eddy Simulation (LES) on a well-resolved mesh. Hence, to carry out these simulations, an in-house higher order ELBM solver [1] was used. The lattice model consists of 167 discrete velocities with the smallest and largest lattice velocities being 0.5 and 3,

respectively. The crystallographic LBM used by the solver improves the capability of LBM by optimally sampling the domain on a Body-Centred Cubic (BCC) lattice instead of the standard Simple Cubic (SC) lattice [14]. The BCC lattice also improves the discretization of geometries in the computational domain. Furthermore, higher-order LB methods have been introduced to extend the applicability over a wider range of Mach and Knudsen numbers. These higher-order models are characterized by improved stability, accuracy and thermal properties [15, 16]. The recently introduced Essentially Entropic LBM [18] ensures the stability of under-resolved simulations, based on the second law of thermodynamics, without any explicit turbulence modelling. This assures an LES like accuracy. The use of ELBM ensures a seamless transition from LES to Direct Numerical Simulation (DNS) based only on increasing the grid resolution without any empirical modelling of small scales.

2. Geometry and Simulation Setup

The geometry, used in the experimental setup[2], is expressed in terms of analytical functions to create the CAD file used by the solver. The computational domain used in the simulations is $15C_r \times 6C_r \times 6C_r$, where C_r is the root chord of the wing measuring 65.364 cm. The streamwise flow direction uses subsonic constant velocity inlet and constant static pressure outlet as boundary conditions while the other directions use the free-slip boundary condition. In order to reduce the use of computational resources, the simulations are performed with a symmetry boundary condition along the longitudinal plane shown in figure 1. The no-slip boundary condition is applied over the surface of the delta wing [19]. A transonic flow Mach number of 0.85 is chosen along with a Reynolds number of 6×10^6, calculated based on the mean aerodynamic chord of 43.576 cm. Simulations are carried out at AoAs of 18.6 and 23.6 degrees, to study the post vortex breakdown scenario.

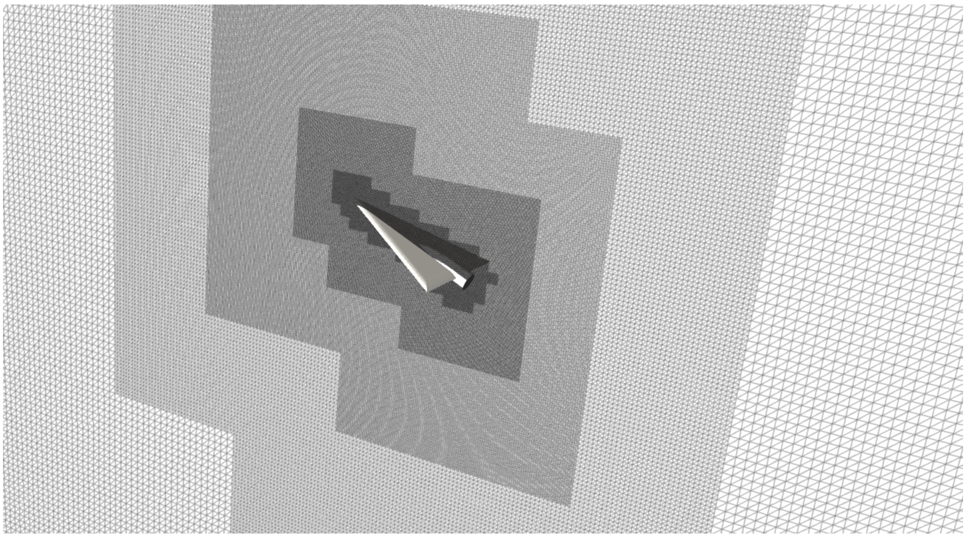

Figure 1 – Multi-resolution grid used for simulation

Figure 1 shows the nine level multi-resolution mesh used for the simulation, where smallest grid resolution is 0.159 mm with a total of 1.2 billion grid points. The grid resolution changes across consecutive levels by a factor of two. Simulations are run for 28 flow convection times based on the root chord length. The total memory used for the simulation is 3.393 TB and 2560 processor cores were used on 40 computing nodes. Each node is configured with two AMD EPYC 7742 processors, containing 512 Gigabytes of Samsung DDR4 3200 MT/s memory and interconnected with high speed Nvidia Mellanox HDR InfiniBand.

3. Results

Qualitative and quantitative comparisons are made with experimental data [2, 17] to understand the phenomenon of shock-vortex interactions with the current solver. The sharp leading edge and the slender body cause the flow to separate early which leads to a primary vortex that dominates the upper surface of the wing. This primary vortex can be observed from the streamlines plotted in

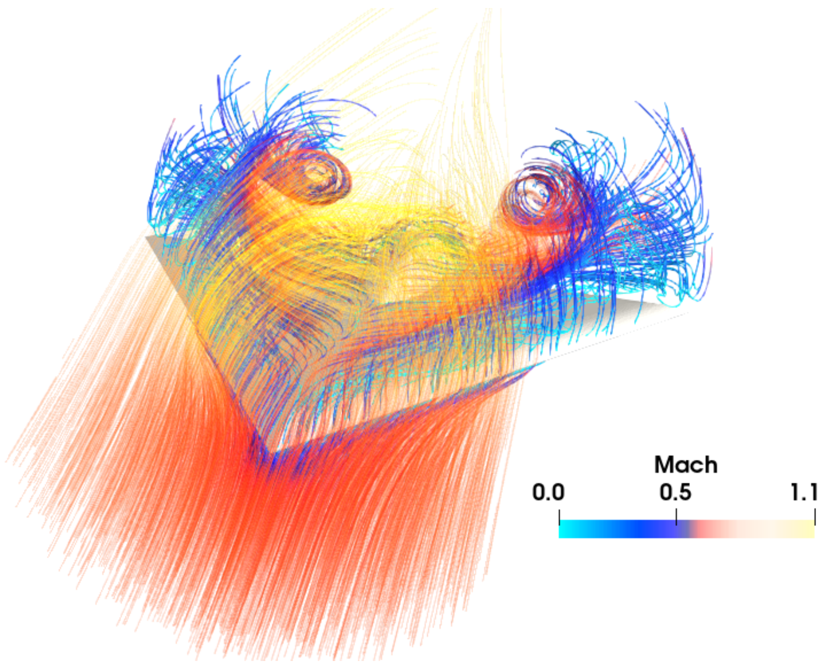

Figure 2 – Streamlines coloured by Mach number capturing the vortical flow and localised supersonic regions over the delta wing

Figure 2. The streamlines in blue show the low-velocity vortical structures at the sharp leading edge and supersonic structures at the core of the primary vortex.

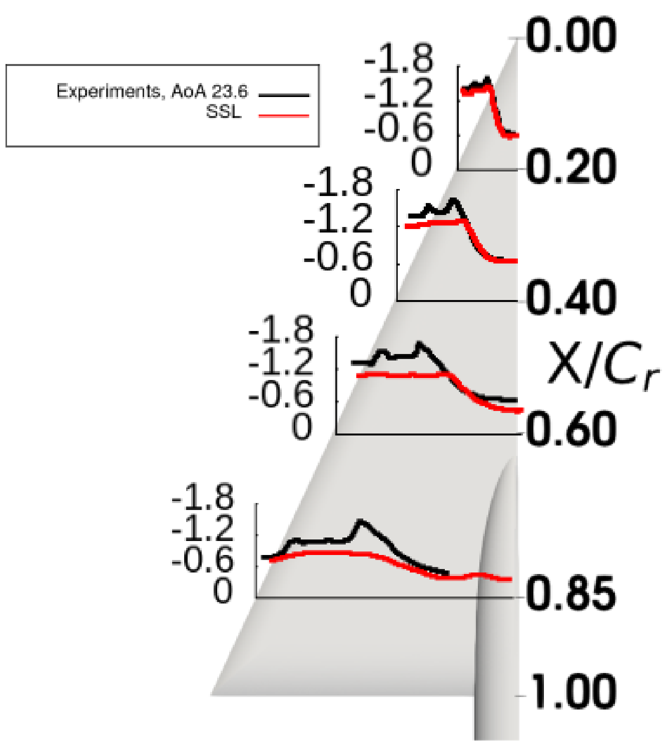

Figure 3 – Coefficient of pressure distribution compared against experimental data [17]

Simulation results are validated by comparing the pressure distribution with experimental data given by [2]. Figure 3 shows the pressure distribution at selected chord wise locations over the wing. These locations are taken in accordance with the experimental data. Simulations show good match in the suction peak close to apex of the wing i.e $x/C_r = 0.2$. Although values further downstream exhibit slight under-prediction, overall pressure distribution matches well when compared with the experiments. The pressure distribution along the leading edge denoted by the corresponding root

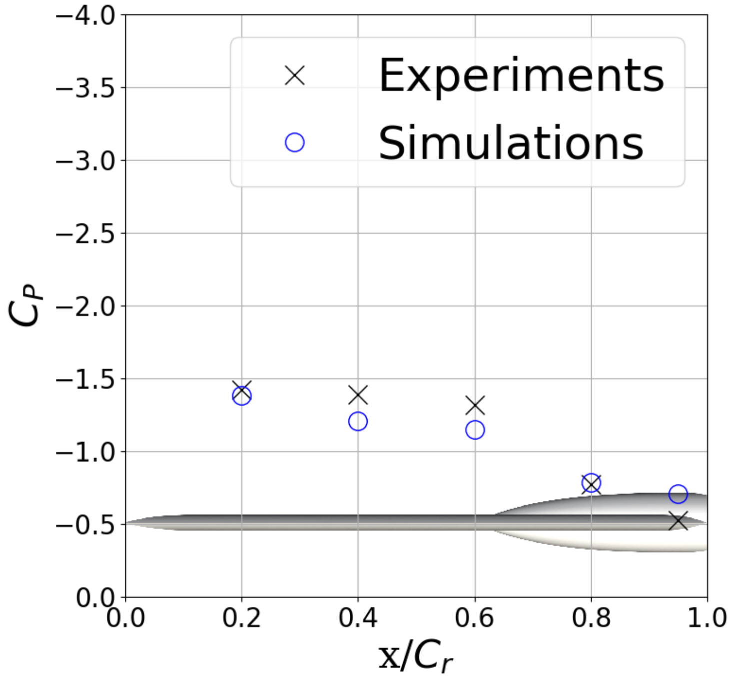

Figure 4 – Coefficient of pressure on upper surface near leading edge along root chord

chord location is plotted in figure 4. These leading edge suction pressure values, which is subset of the earlier figure 3, agree well with the reference data. The computed value of normal force coefficient from the simulation is 0.975 as compared to the experimental value of 1.0295.

3.1 Vortex Breakdown

As mentioned earlier, the vortex breakdown is expected to occur beyond 22° AoA and its location along the chord in the symmetrical plane (x/C_r) is close to 0.6. We performed simulations at 18.6°and 23.6°to capture the effects of vortex breakdown with the current solver. Mach number contours are

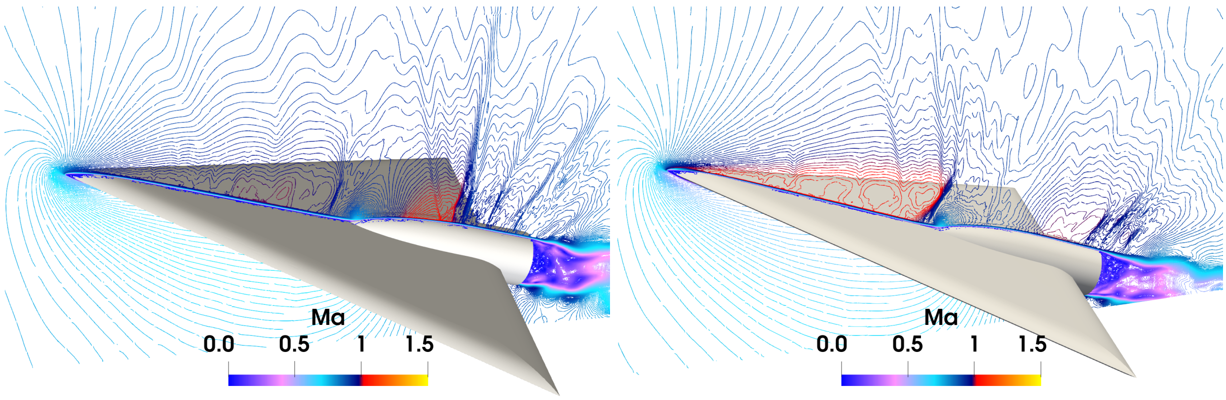

(a) AoA 18.6° (b) AoA 23.6°

Figure 5 – Mach number distribution at the plane of symmetry

plotted on the symmetry plane of the wing in figure 5. Clustering of contours in figure 5b near

the upstream of the sting tip indicates the presence of a normal shock approximately located near $x/C_r = 0.6$. Another shock towards the rear end of the wing can also be seen. The location of the normal shock in figure 5a is observed further downstream towards the rear end of the sting.
To understand the shock structures in the flow, mach contours along the spanwise direction on planes at different x/C_r locations are plotted. Fig 6 shows the Mach number contours for both angles of attack. A specific color palette was chosen to identify the supersonic region. It can be observed in the fig 6 that the velocity near the core of the primary vortex drops between the slice $x/Cr = 0.6$ and $x/Cr = 0.8$ with AoA 23.6°, however with AoA of 18.6°it continues to be supersonic region and does not show a vast reduction of velocity. The size of the primary vortex is also larger in the downstream with AoA 23.6°than compared with AoA 18.6°. This shows the breakdown of vortex in the region very close to $x/C_r = 0.6$ in the 23.6°case, along with the presence of normal shock evident from the pressure distribution in figure 5 very close to the sting tip. Hence, a shock vortex interaction can be inferred from this data, which may also has a role to play in the breakdown of the vortex.

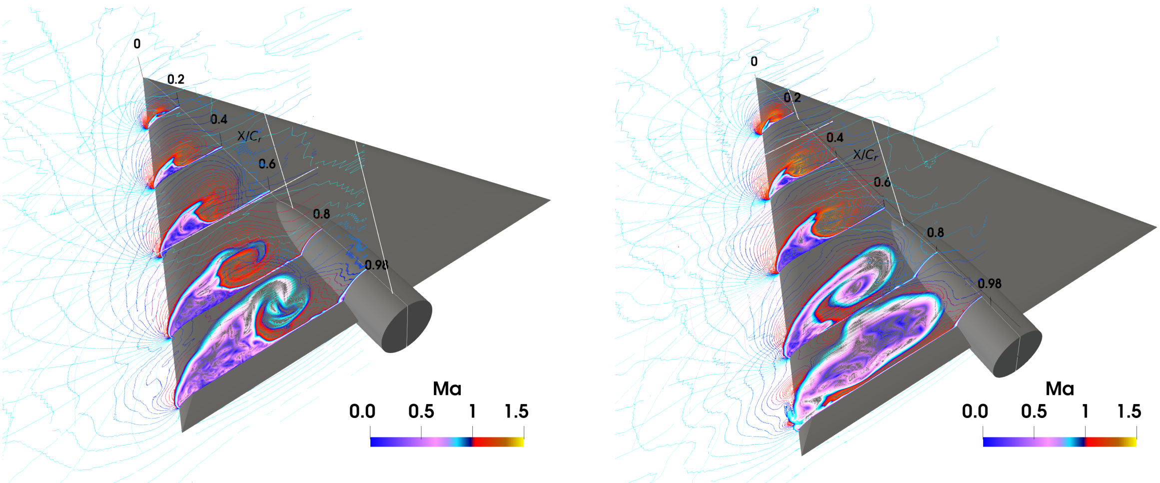

(a) AoA 18.6°

(b) AoA 23.6°

Figure 6 – Mach number contours along span at various chord-wise locations

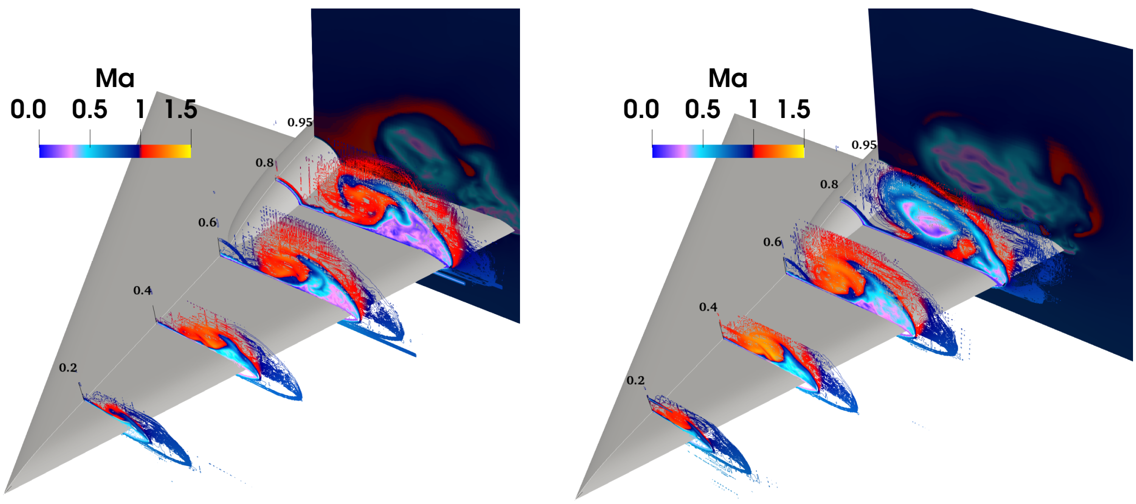

(a) AoA 18.6°

(b) AoA 23.6°

Figure 7 – Iso-contours of vorticity plotted along the span at different streamwise locations

In order to observe the primary vortex closely, we have plotted the iso-contours of the streamwise component of vorticity on planes along the wing span at different chord sections as shown in Figure 7. The contours in figure 7 are coloured with the Mach number in order to trace the supersonic patches in the flow. This highlights the vortical flow structures along with their corresponding Mach number showing possible interactions in the shock-vortex system. It also shows the evidence of cross-flow shocks present in the flow. The secondary and tertiary separation underneath the primary vortex is well captured and are more dominant in the rear portion of the wing. As the local flow becomes supersonic, shock waves appear between the primary and secondary vortices. These shock waves gives rise to complex interactions between the shock-vortex system.

4. Summary

Flow past a sharp leading edge delta wing in the transonic regime is simulated using the SankhyaSutra Labs© ELBM solver. The surface pressure distribution along span at different chord locations is compared with experimental results for validation. The coefficient of pressure near the leading edge at various chord locations is also reported against experimental calculations. Primary vortex structures over the wing are visualised using velocity streamlines. Mach contours on the symmetry plane show evidence of normal shock upstream of the sting tip. Mach contours at various chord sections of the wing are plotted to show the vortex breakdown with angle of attack of 23.6°in the region near to the sting tip. Iso-contours of vorticity along the span at different locations over the chord before and after critical vortex breakdown angle is plotted.

5. Conclusion

Thus, transonic ELBM can be used to analyse vortical systems and shock structures of flow over a delta wing without the use of any explicit turbulence models. The current solver has captured the pressure losses, secondary vortex structures and the presence of terminating and cross-flow shocks over the wing planform.

References

[1] Hanumantharayappa, M. N., Thantanapally, C., Namburi, M., Kumaran, V., and Ansumali, S. (2021). LES/DNS of flow past T106 LPT cascade using a higher-order LB model. *In AIAA Propulsion and Energy 2021* Forum (p. 3485).

[2] Chu, Julio. Experimental surface pressure data obtained on 65 delta wing across Reynolds number and Mach number ranges. Vol. 3. *National Aeronautics and Space Administration*, Langley Research Center, 1996.

[3] Donohoe, S. R. and Bannink, W. J., "Surface Reflective Visualisations of Shock-wave/Vortex Interactions Above a Delta Wing," *AIAA Journal* , Vol. 35, No. 10, 1997, pp. 1568-1573

[4] Escudier, M., "Vortex Breakdown: Observations and Explanations," *Progress in Aerospace Sciences*, Vol. 25, 1988, pp. 189-229.

[5] Hoeijmakers, H. W. M., "Modelling and Numerical Simulation of Vortex Flow in Aerodynamics" AGARD Conference Proceedings "Vortex Flow Aerodynamics", *AGARD-CP-494*, July 1991, pp. 1.1-1.46.

[6] Deléry, J. M., "Physics of Vortical Flows", *Journal of Aircraft*, Vol. 29, No. 5, 1992, pp. 856-876.

[7] Deléry, J. M., "Aspects of Vortex Breakdown," *Progress in Aerospace Sciences*, Vol. 30, No. 1, 1994, pp. 1-59

[8] Gursul, I., "Recent Developments in Delta Wing Aerodynamics," *Aeronautical Journal*, 2004, pp. 437-452

[9] Schiavetta, Lucy and Boelens, Okko and Fritz, Willy. Analysis of transonic flow on a slender delta wing using CFD *24th AIAA Applied Aerodynamics Conference*, p 3171 , 2006

[10] Kandil, O. A., Kandil, H. A., and Liu, C. H., “Shock-Vortex Interaction over a 65-degree Delta Wing in Transonic Flow,” *AIAA 24th Fluid Dynamics Conference, AIAA-93-2973*, July 1993

[11] Erickson, G., Schreiner, J., and Rogers, L., “Multiple Vortex and Shock Interactions at Subsonic,Transonic and Supersonic Speeds,” *AIAA*-90-3023, 1990

[12] Elsenaar, A., Hjemberg, L., Bütefisch, K. A., and Bannink, W. J., “The International Vortex Flow Experiment,” Validation of Computational Fluid Dynamics - *AGARD-CP-437 Volume 1* , AGARD, 1988, pp. 9.1–9.23.

[13] Erickson, G. E. and Rogers, L. W., “Experimental Study of the Vortex Flow Behaviour on a Generic Fighter Wing at Subsonic and Transonic Speeds,” *19th AIAA Fluid Dynamics, Plasma Dynamics and Lasers Conference, AIAA-87-1262* , June 1987.

[14] Namburi, M., Krithivasan, S., and Ansumali, S., "Crystallographic lattice Boltzmann method," *Scientific reports*, Vol. 6, No. 1,2016, pp. 1-10

[15] Kolluru, P. K., Atif, M., Namburi, M., and Ansumali, S., "Lattice Boltzmann model for weakly compressible flows" *PhysicalReview E*, Vol. 101, No. 1, 2020, p. 013309

[16] Atif, M., Namburi, M., and Ansumali, S., "Higher-order lattice Boltzmann model for thermohydrodynamics," *Physical ReviewE*, Vol. 98, No. 5, 2018, p. 053311

[17] Elsenaar, A. and Hoeijmakers, H. W. M., "An Experimental Study of the Flow over a Sharp-Edged Delta Wing at Subsonic and Transonic Speeds," *AGARD Conference Proceedings "Vortex Flow Aerodynamics"* , AGARD-CP-494, July 1991, pp. 15.1-15.19.

[18] Atif, M., Kolluru, P. K., Thantanapally, C., and Ansumali, S. (2017). Essentially entropic lattice Boltzmann model. *Physical review letters*, 119(24), 240602.

[19] Krithivasan, Siddharth, Siddhant Wahal, and Santosh Ansumali. "Diffused bounce-back condition and refill algorithm for the lattice Boltzmann method." *Physical Review E* , 89.3 (2014): 033313.

[20] Houtman, E. M., Bannink, W. J. ."Experimental and numerical investigation of the vortex flow over a delta wing at transonic speed." *AGARD, Vortex Flow Aerodynamics 11 p(SEE N 92-12996 04-02).* , (1991)

6. Copyright Statement